Expansivity of fused quartz glass measured within 6×10^{-10} /K

Patrick F. Egan[a)]
National Institute of Standards and Technology, 100 Bureau Dr, Gaithersburg, MD 20899

(Received 14 September 2022; Accepted 25 November 2022;
Published 20 December 2023)

Thermal expansion sometimes dominates uncertainty in a precision measurement. A cell-based refractometer has been designed at NIST which targets 10^{-6} relative uncertainty in the measurement of helium refractivity; in terms of absolute refractive index at ambient conditions, the accuracy goal is 3×10^{-11}. To achieve this level of accuracy, the length of a 0.5 m gas cell would need to be known within 100 nm. This is achievable when cell length is measured by coordinate-measuring machine at 20 °C. However, the refractometer will operate at the thermodynamically known fixed-points of water and gallium, near 0 °C and 30 °C, respectively. The cell is made from fused quartz glass, which has a nominal thermal expansion coefficient of 0.4 (µm/m)/K. Therefore, to scale the accuracy of the dimensional metrology across 20 °C to the triple-point of water requires that the thermal expansion coefficient of fused quartz glass is known within 10 (nm/m)/K, or 2.5 %.

A method is described to measure the thermal expansion coefficient of fused quartz glass. The measurement principle is to monitor the change in resonance frequency of a Fabry–Perot cavity as its temperature changes; the Fabry–Perot cavity is made from fused quartz glass. The standard uncertainty in the measurement was less than 0.6 (nm/m)/K, or 0.15 %. The limit on performance is arguably uncertainty in the reflection phase-shift temperature dependence, because neither thermooptic nor thermal expansion coefficients of thinfilm coatings are reliably known. However, several other uncertainty contributors are at the same level of magnitude, and so any improvement in performance would entail significant effort. Furthermore, measurements of three different samples revealed that material inhomogeneity leads to differences in the effective thermal expansion coefficient of fused quartz; inhomogeneity in thermal expansion among samples is 24 times larger than the measurement uncertainty in a single sample.

I. INTRODUCTION AND MOTIVATION

An experimental effort is underway to measure the refractivity of helium gas at the level of $10^{-6} \cdot (n-1)$. The motivation is that a precision measurement of helium refractivity at known temperature allows a realization of the pascal, in what is sometimes called the optical pressure scale[1]. The underlying principle is the ideal gas law, which defines pressure $p = \rho RT$ in terms of density ρ and temperature T; the gas constant R is a fixed value. The interest in helium (refractivity) is because the Lorentz–Lorenz equation provides a direct link between refractivity and density $\rho = \frac{2}{3A_R}(n-1) + \cdots$ via the polarizability A_R. Polarizability is a fundamental property of a single atom, and for helium, it may be calculated[2] well within $10^{-6} \cdot A_R$. Consequently, the realization $p = \frac{2}{3A_R}(n-1)RT$ provides a well-understood physical system, in which all input parameters are known without reference to an ancillary measurement of pressure. The ultimate accuracy of this new scale approaches the $u(T)$-limit; or, how well the thermodynamic temperature of the helium gas is known.

a)Electronic mail: egan@nist.gov

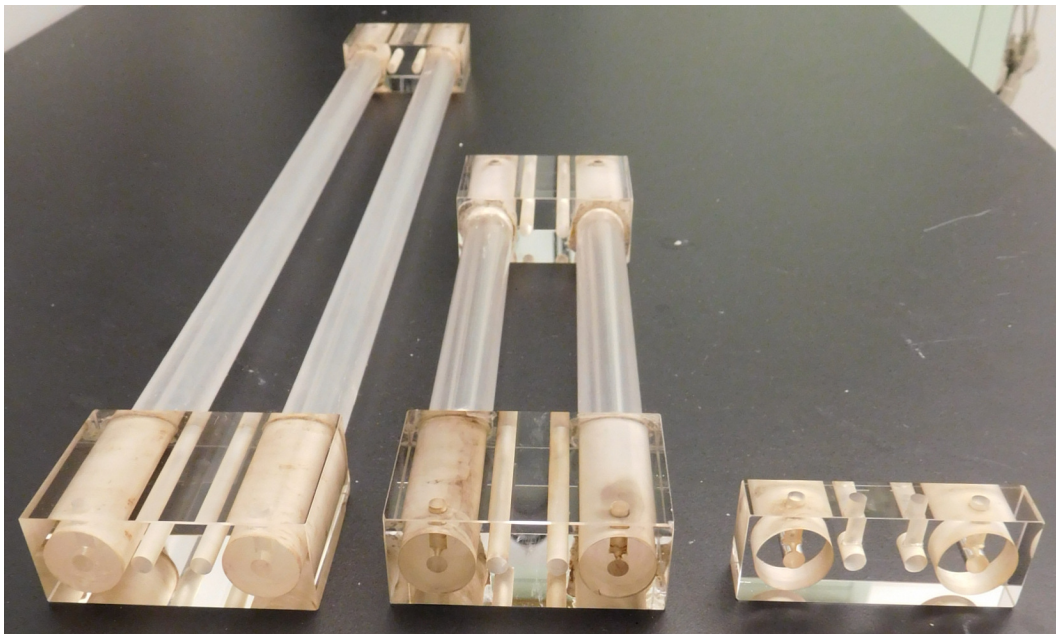

FIG. 1. The three gas cells have been manufactured by potting precision-bore fused quartz glass tubing into end blocks. Cell lengths are 500 mm, 258 mm, and 15 mm. Cell lengths should be dimensioned before the windows are bonded to the assembly.

To measure refractivity, an approach based on gas cells is being pursued. The scheme closely follows the effort of Egan *et al.*[3] to determine the Boltzmann constant, with the working principle of making window pathlength error common-mode in measurements of refractivity performed in cells of different length. Two design tweaks have improved the concept of Ref. 3: the cells and windows have been made in fused quartz glass, and the length of the long cell is 0.5 m. These two design tweaks should achieve (uncorrected) window pathlength error at $90 \times 10^{-6} \cdot (n-1)$ for helium, and common-mode cancellation techniques are expected to reduce this by more than an order-of-magnitude. The long, medium, and short cells are photographed in Figure 1.

At these expected levels of accuracy, uncertainty in gas temperature will become the dominant contribution to uncertainty in $p = \frac{2}{3A_R}(n-1)RT$. Therefore, the helium measurements will be performed with direct thermometry comparisons to the fixed-points of water and gallium, at 0.01 °C and 29.76 °C, respectively. However, cell length is determined by coordinate measurement, which is performed at the 20 °C reference temperature of dimensional metrology. The objective is to scale the dimensional measurements across 20 °C and hold 100 nm, which would correspond to fractional error of $0.2 \times 10^{-6} \cdot (n-1)$ in the cell-based refractometer. Since the coefficient of thermal expansion (CTE) of fused quartz glass is approximately 0.4 (µm/m)/K, holding a 0.5 m dimension across 20 K within 100 nm requires knowledge of CTE within 10 (nm/m)/K, or 2.5 %.

Vitreous silica was a standard reference material for thermal expansion for many decades[4]. However, the glass exhibits variations in its CTE, which have been attributed to recipe, process preparation, and thermal history[4–7]. The cell assemblies of Figure 1 are made with tubes of Type-I electric-fusion quartz glass. However, the thick wall tubes were made of a lamination of an inner and outer tube, and one therefore is not certain of the thermal history of the material. The windows on the cell assemblies are Type-III synthetic fused silica glass (colloquially known as UV-grade fused silica). Wang, Yamada, and Okaji[8] show variations in $\int \alpha(T)\,\mathrm{d}T \equiv \frac{\Delta L}{L}$ less than 1 µm/m between Type-I and Type-III glasses across 0.01 °C to 29.766 °C, but material mismatch might cause a small end effect. Another more important potential end-effect is that the tubes are bonded into end-blocks with a potting

compound. The potting compound is a paste of silica powder, mixed with monoaluminum phosphate solution; the tubes were potted into the end blocks with a slip fit of 50 µm, and fired to 300 °C for 24 h. The potting compound has a generic mean CTE specification of 0.59×10^{-6} /K. Based on these circumstances and a potential mismatch in expansion, it was considered critical to measure the CTE of a "mock cell" sample, upon which to base the estimate of the effective CTE of the cell assembly.

II. MEASUREMENT APPROACH

The situation is that the lengths of the cells are measured by coordinate-measuring machine at a reference temperature $T_{\mathrm{ref}} = 293.15$ K. The actual cell length at the refractometry working temperature $T_{\mathrm{TPW}} = 273.16$ K requires that the measured length L_{ref} (i.e., L_{CMM}) is corrected

$$L = L_{\mathrm{ref}} \left[1 + \int_{T_{\mathrm{ref}}}^{T_{\mathrm{TPW}}} \alpha_{\mathrm{cell}}(T)\, \mathrm{d}T \right] \tag{1}$$

for the thermal expansion coefficient $\alpha_{\mathrm{cell}}(T)$, which is the unknown.

The mock cell samples used to infer $\alpha_{\mathrm{cell}}(T)$ are Fabry–Perot (FP) cavities, which have spacers made from tubes of the same material batch as used in the cell assemblies; that is, Type-I fused quartz glass. The FP cavities were formed by polishing the end faces of the tubes parallel, and silicate-bonding mirrors to each end. The measurement principle[9] is to track changes in the resonance frequency of each cavity as a function of temperature, relative to the reference frequency of an iodine-stabilized laser. As such, the metrology scheme closely resembles that of Ref. 10, comprising a pair of tunable HeNe lasers, dither-locked to the resonance peaks of each cavity, and some frequency metrology. The metrology assembly is sketched in Figure 2, and is entirely high-vacuum compatible. The two FP cavities were placed side by side in their own suspension frame enclosure, and were suspended by 0.3 mm diameter cable at their Airy-points. The temperature of each aluminum suspension enclosure was measured with a thermistor embedded in a thermowell. These two thermistors had been calibrated on the international temperature scale of 1990 (ITS-90) relative to a standard platinum resistance thermometer. The apparatus of Figure 2 was placed in a vacuum chamber and submerged in a 150 L stirred water bath; fiber inputs and outputs were fed through the water and chamber. This paragraph completes the basic description of the method—the change in resonance frequency of the tube cavities was measured as a function of temperature—further details are left to Ref. 10.

The (approximate) resonance frequency of a FP cavity at vacuum, $\nu \approx \frac{mc}{2L}$, depends on cavity length L and the integer mode number m; the speed of light in vacuum c is a constant. Consequently, changes in the length of the cavity may be inferred by measuring the change in resonant frequency via the difference equation $\frac{\mathrm{d}L}{L} = -\frac{\mathrm{d}\nu}{\nu}$, while updating $\mathrm{d}\nu$ for the change in mode number Δm, caused by the changes in cavity temperature. (In these measurements, $\frac{\mathrm{d}\nu}{\mathrm{d}T} \approx 180$ MHz/K. For the 50 K change in the long cavity temperature, $\Delta m = 30$.) From the inferred specimen (cavity) length as a function of temperature $L(T)$, one may deduce the instantaneous CTE $\alpha(T) = \frac{1}{L_{\mathrm{ref}}} \frac{\mathrm{d}L}{\mathrm{d}T}$. Since this experiment deals with specimens of different lengths, it is expedient to fit fractional length $\frac{L(T)}{L_{\mathrm{ref}}} = a_0 + \sum_{i=1}^{3} \frac{a_i}{i} (T - T_{\mathrm{ref}})^i$ about the reference temperature $T_{\mathrm{ref}} = 293.15$ K. The resulting fit coefficients then describe instantaneous CTE as a functional approximation

$$\alpha(T) = \sum_{i=1}^{3} a_i (T - T_{\mathrm{ref}})^{i-1}. \tag{2}$$

This simplified treatment has ignored the temperature-dependent effects in diffraction and mirror phase shift on reflection—the latter has a temperature dependence which is non-negligible, and will be discussed in the uncertainty section below.

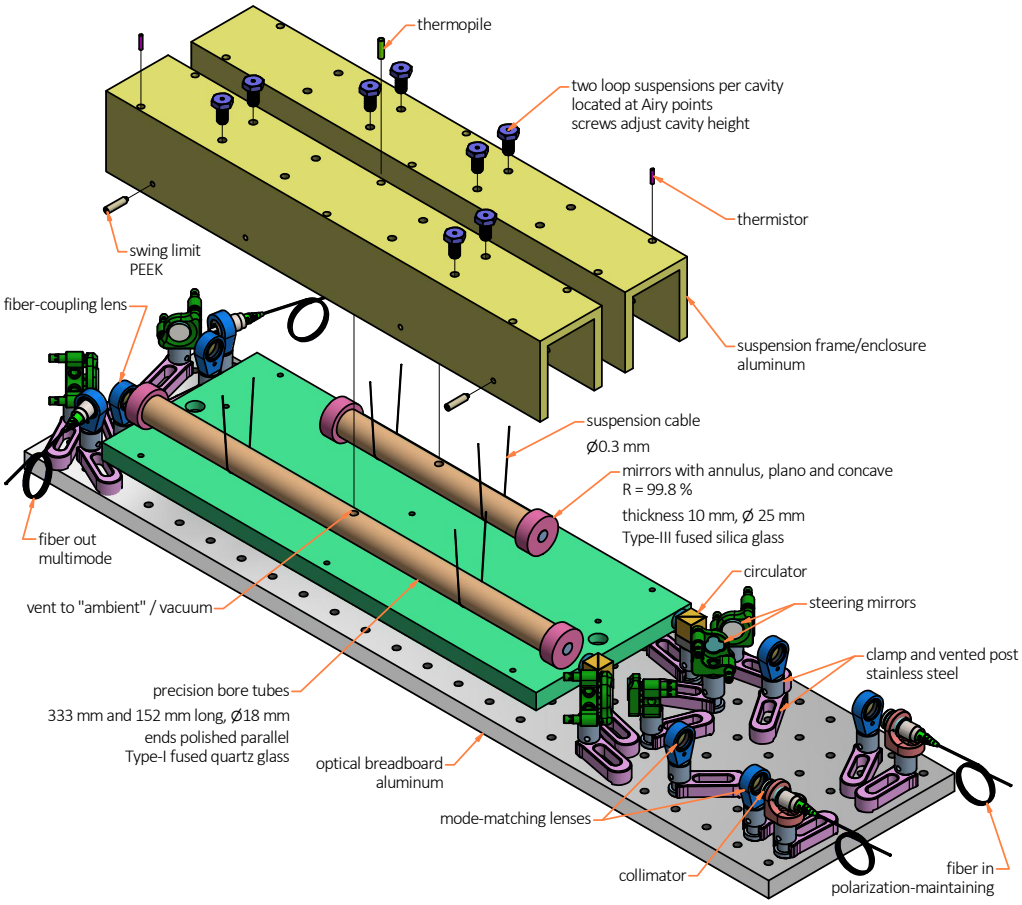

FIG. 2. Setup for the thermal-expansion measurement. Two Fabry–Perot cavities were formed out of excess (cell) tubing material, and suspended side by side. The sketched assembly was placed inside an inner shell and vacuum chamber, which was submerged in a water bath. Temperature of the water bath was varied between −10 °C and 40 °C.

A. Results for Two Sets of CTE Measurements

Two sets of CTE measurements were performed. The first set cycled the cavities $\mathrm{FP}_{152}^{\text{Type-I}}$ and $\mathrm{FP}_{333}^{\text{Type-I}}$ side by side, and the second set cycled $\mathrm{FP}_{152}^{\text{potted}}$ and $\mathrm{FP}_{333}^{\text{Type-I}}$ side by side. For the second set, the 152 mm cavity had been potted with slip-fit tubes, while the 333 mm cavity remained unchanged between the two sets of measurements. This second set of measurements is the basis for the estimate $\alpha_{\text{cell}}(T)$.

In Figure 3(a) both sets of measurements are plotted as fractional change in cavity length as a function of temperature. For each cavity, the $\frac{L(T)}{L_{\text{ref}}}$ dataset was regressed to a cubic function, and produced coefficients specific to each cavity. The question of how much these sets of coefficients differed from one another is best answered by the diagnostic described in the next paragraph. Figure 3(b) shows residuals from the fits to fractional length, where the ordinate corresponds to $\frac{L(T)}{L_{\text{ref}}} - [a_0 + \sum_{i=1}^{3} \frac{a_i}{i}(T - T_{\text{ref}})^i]$. The plot shows residuals on the specimens $\mathrm{FP}_{152}^{\text{Type-I}}$ and $\mathrm{FP}_{333}^{\text{Type-I}}$ from the first measurement set, and specimen $\mathrm{FP}_{152}^{\text{potted}}$ from the second measurement set. (For clarity in Figure 3, the second measurement set for $\mathrm{FP}_{333}^{\text{Type-I}}$ is not shown. Using the metric $\int \alpha(T)\,\mathrm{d}T$, the two measurements of $\mathrm{FP}_{333}^{\text{Type-I}}$ reproduce within 0.7 nm/m across the 50 K range.) The root-mean-square error from the

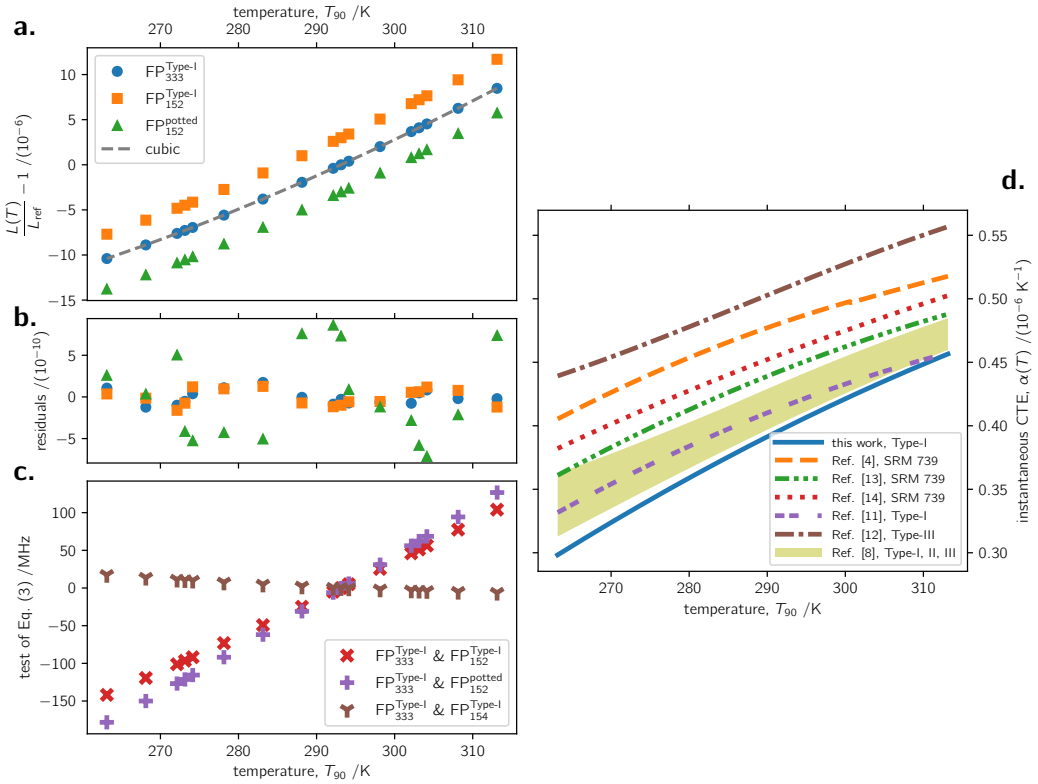

FIG. 3. (a) Change in fractional cavity length as a function of temperature for Type-I fused quartz glass $\mathrm{FP}_{333}^{\text{Type-I}}$ and $\mathrm{FP}_{152}^{\text{Type-I}}$, and the potting-compound-modified $\mathrm{FP}_{152}^{\text{potted}}$. The plots are offset by 3×10^{-6} in the ordinate for clarity. (b) Residuals from the fit: the $\frac{L(T)}{L_{\text{ref}}}$ dataset for each FP cavity has its own fit coefficients. (c) Anomalous change in the intercavity beat frequency, defined as Eq. (3). The slope of the trends is proportional to inhomogeneity $\Delta\alpha \approx \frac{1}{\nu}\frac{\Delta f_{\text{beat}}}{\Delta T}$ between the specimens being compared. (d) The deduced thermal expansion for Type-I fused quartz glass, as Eq. (2) in this work. Literature measurements also shown.

fits of the first measurement set are 82 pm/m for $\mathrm{FP}_{333}^{\text{Type-I}}$ and 94 pm/m for $\mathrm{FP}_{152}^{\text{Type-I}}$. The residuals for $\mathrm{FP}_{152}^{\text{potted}}$ are 5.5 times larger than $\mathrm{FP}_{152}^{\text{Type-I}}$, which is most likely an increase in cavity instability caused by the potting compound, because the $\mathrm{FP}_{333}^{\text{Type-I}}$ residuals for the second set of measurements are within 15 % of the first set—it is no surprise that a potting compound increases instability compared to bulk material. The fit residuals for long and short cavities show obvious correlation, and the shape of the residuals persists in both sets of measurements, which suggests a systematic error affecting the length of both cavities during the measurement cycle. The most likely cause for the correlated residuals is error in thermometry, on the order of $\delta T = \frac{1}{\alpha}\frac{\delta L}{L} \approx 0.3$ mK.

A key experimental diagnostic is the intercavity beat: that is, the < 1 GHz difference in frequency between the two lasers locked to a resonance frequency in each cavity. For cavities of identical material properties experiencing identical temperature changes, the intercavity beat would remain constant as a function of temperature. Stated more precisely,

$$f_{\text{f}} - \frac{f_{\text{ref}} + \left(\dfrac{\Delta m_{33} \cdot c}{2L_{33}} - \dfrac{\Delta m_{15} \cdot c}{2L_{15}}\right)}{1 + \displaystyle\int_{T_{\text{ref}}}^{T_{\text{f}}} \alpha(T)\,\mathrm{d}T} \stackrel{?}{=} 0. \tag{3}$$

Or, the change in intercavity beat measured at two different temperatures $T_{\text{ref}} < T_{\text{f}}$—when

adjusted for changes in mode order of the respective cavities and scaled for their increasing length—should be zero, if the cavities have the same coefficient of thermal expansion, experience the same temperature change, and have no end effect. Figure 3(c) belies these assumptions and the potential equality of Eq. (3), demonstrating a linear trend of about 4.9 MHz/K in the case of $\mathrm{FP}_{152}^{\text{Type-I}}$ and $\mathrm{FP}_{333}^{\text{Type-I}}$ dataset. A temperature-related explanation for the trend is implausible—it would require an undetected change in gradient between the cavities of 1.25 K, which is more than three orders of magnitude larger than what was measured. Two considered end effects are a mismatch in CTE between the tube and mirror substrates, and a temperature dependence on cavity round-trip phase. Combined, these two end effects are about a factor 30 too small to explain the changing intercavity beat. Therefore, the most likely explanation behind the trend of Figure 3(c) is inhomogeneity in the CTE of fused quartz glass among different tubes, corresponding to $\Delta\alpha \approx \frac{1}{\nu}\frac{\Delta f_{\text{beat}}}{\Delta T}$, or 1.1×10^{-8} /K. The magnitude of this inhomogeneity—2.5 %—is somewhat surprising, but should be placed in context of a thorough work by Jacobs, Shough, and Connors[11], which compared thirteen different samples of fused quartz glass, core-drilled from distant locations in four separate ingots (glass melts). These authors showed a location-dependent gradient in $\alpha(T)$ across each ingot, and they stated that the maximum variation in $\alpha(T)$ among three of the four melts was 5×10^{-9} /K. They chose to "remove" data from the fourth melt because "a different grade of crystalline quartz [was] used to yield a reduced bubble content." Nevertheless, this fourth melt would still be classified as a Type-I fused quartz glass, and if it is included in the data analysis, Jacobs, Shough, and Connors[11] showed variations in $\alpha(T)$ of up to 1.3×10^{-8} /K among the thirteen samples from four separate melts. (See, in particular, their Figure 13.) The CTE inhomogeneity of the present result in Figure 3(c) is therefore not too surprising. However, the present result for absolute CTE in both specimens, discussed next, also requires mediation. [For purposes of the uncertainty evaluation which follows in the next section, a third specimen $\mathrm{FP}_{154}^{\text{Type-I}}$ of the same material was constructed. It is shown in Figure 3(c) that $\mathrm{FP}_{154}^{\text{Type-I}}$ has close agreement in $\alpha(T)$ to the specimen $\mathrm{FP}_{333}^{\text{Type-I}}$. The relevance of this result is discussed more in the uncertainty section.]

In Figure 3(d) is plotted $\alpha(T)$ deduced from these measurements, expressed by Eq. (2). The present measurements are compared with the existing literature[4,8,11–14] in this temperature range. There are at least four notable aspects to the literature, interpreted through the following anecdotal commentary:

- The first is evident in Figure 3(d) as the difference between the trends "Ref. 4, SRM 739," "Ref. 13, SRM 739," and "Ref. 14, SRM 739." Okaji and coworkers have consistently reported[8,14] a bias of 2×10^{-8} /K to 3×10^{-8} /K between their measurements of SRM 739 versus what was originally reported by Hahn and Kirby[4]. This bias is within the mutual standard uncertainties for $\alpha(T)$, which was 3×10^{-8} /K for Hahn and Kirby and 2×10^{-8} /K for Okaji and coworkers. Drotning[13], whose measurements of $\alpha(T)$ in SRM 739 are also lower than Hahn and Kirby, does not make a clear uncertainty statement, but says that the 2.7×10^{-8} /K standard deviation on their measurements was "near the estimated device uncertainty." The anecdotal conclusion of this first point is that the measurement of Hahn and Kirby[4] overestimates $\alpha(T)$ for SRM 739.

- The second notable feature of Figure 3(d) is the offset between data for SRM 739 compared to the shaded area plot of "Ref. 8, Type-I, II, III" which covers the range of fit data reported for all types of vitreous silica glass measured by Wang, Yamada, and Okaji[8]. This offset is notable because SRM 739 is nominally a Type-I fused quartz glass, and yet its thermal expansion coefficient (i.e., Ref. 14) is outside the range of silica glasses investigated by Wang, Yamada, and Okaji, and measured with the same apparatus. The origin of this offset is not clear, but Wang, Yamada, and Okaji suggest that it may be related to the manufacturing process. (A subsequent article by the same Okaji group[15] extends the valid temperature range, and its findings are consistent with Refs. 8 and 14.) The anecdotal conclusion of this second point is that

the recipe, process, or preparation of SRM 739 produces a Type-I fused quartz glass with $\alpha(T)$ relatively higher than other Type-I glasses.

- The third notable aspect of Figure 3(d) is the 9×10^{-8} /K offset between Ref. 12 and Ref. 8 for Type-III fused silica glass; when these two Groups performed a bilateral comparison[16] with the same SRM 739 specimen, they had agreement within 2×10^{-8} /K, and claimed standard uncertainties on the order of 0.9×10^{-8} /K. The anecdotal conclusion of this third point is that the same process or preparation (of Type-III fused silica glass) may produce variability as large as the range of all data in Figure 3(d).

- Finally, the work of Jacobs, Shough, and Connors[11] should be mentioned. (Ref. 11 does not list fit coefficients, but a plot digitizer[17] was used to interpolate their Figure 1.) Jacobs and coworkers pioneered the FP cavity based approach to CTE measurement for at least three decades[9,11,18–20]. Arguably, Ref. 11 was the acme in their body of work; in Ref. 11 they demonstrate reproducibility at the level of 1×10^{-9} /K, and make a thermometry-limited uncertainty claim of 4.5×10^{-9} /K in the measurement of a Type-I fused quartz glass. The anecdotal conclusion of this fourth point is that the hitherto most accurate claim on $\alpha(T)$ for a Type-I fused quartz glass is notably lower than older data in Figure 3(d).

- Parenthetically, also mentioned are two older sets of measurements which are not plotted in Figure 3(d). Berthold and Jacobs[18] do not give fit coefficients, but their $\alpha(T)$ plot for a Type-III specimen appears in good agreement with the Type-III measurements of Birch[12]; however, despite claimed precision of 1×10^{-9} /K, one of Berthold and Jacobs' three specimens differed by 4×10^{-8} /K from the others. The second older measurement for a Type-III specimen was by Bennett[21], and is also in good agreement with Birch[12]; however, Bennett's result for a Type-I specimen is 4×10^{-8} /K below the shaded area Wang, Yamada, and Okaji[8]; at 293.15 K, Bennett reports a difference in $\alpha(T)$ of 15×10^{-8} /K between Type-I and Type-III silica glasses.

Taken together, the preceding comments about the literature and Figure 3(d) convey what motivated the present CTE measurements of fused quartz glass: neither measurements on the same glass recipe nor estimates of variability among recipes appear reliable at the ±10 % level in the temperature range of interest ($273 < T < 303$) K. Despite these staging remarks, the present measurement result for $\alpha(T)$ is no less surprising: the present work is clearly "on the low side," and furthermore, the claimed uncertainty is 5.4×10^{-10} /K, or 0.15 %. It is a struggle to coherently place the present "low" measurement in the context of historical reports. Regarding the Type-I fused quartz glass SRM 739, mutual consistency may only be claimed with the work of Drotning[13]; the present result is approximately $2.9u$ lower than Okaji and coworkers[14], and $2.7u$ lower than the foundational work of Hahn and Kirby[4]. [Here, u refers to the combined standard uncertainty of two measurements, and the quantity being compared is $\int_{263}^{313} \alpha(T)\, \mathrm{d}T$.] It is emphasized that the Type-I definition into which the tube material and SRM 739 are categorized is nominal, and it therefore may be misleading to read too much into discrepant results. Moreover, Okaji and coworkers' most recent measurements[8] cover five different recipes of fused quartz glass including Type-I, compared to which they find $\alpha(T)$ of SRM 739 to be anomalously high. Notably, the present result is mutually consistent with all five recipes reported by Okaji and coworkers[8,15], encompassing Type-I, II, III silica glasses. Finally, it appears that the hitherto most accurate claim on a CTE measurement for a Type-I fused quartz glass was by Jacobs, Shough, and Connors[11]: the present measurements are only consistent with Ref. 11 above 295 K, if allowance is made for the 2 % to 3 % inhomogeneity observed in both cases.

A summary of the CTE measurements for all specimens in this work is presented in Table I. The stated uncertainties on the fit parameters are statistical only, and refer to the square-root of the diagonal elements in the covariance matrix. The combined standard uncertainty for the measurement of $\alpha(T)$ is described in the next section. Acknowledging the observed inhomogeneity (imperfect reference material), these CTE measurements are among

TABLE I. Fit coefficients for Eq. (2) measured for each specimen, valid in the range ($263.15 < T_{90} < 313.15$) K for $p < 40$ mPa. Numbers in brackets are statistical uncertainty only. The recommended coefficients are the weighted-average for all three Type-I specimens measured.

specimen	a_1 /(10^{-7} K^{-1})	a_2 /(10^{-9} K^{-2})	a_3 /(10^{-11} K^{-3})	$\frac{\Delta L}{L} = \int_{263}^{313} \alpha(T)\,\mathrm{d}T$ /(10^{-6})
$\mathrm{FP}_{333}^{\text{Type-I}}$	3.95775(4)	3.0146(4)	−1.299(3)	18.86
$\mathrm{FP}_{152}^{\text{Type-I}}$	4.06378(4)	3.0544(5)	−1.306(3)	19.38
$\mathrm{FP}_{152}^{\text{potted}}$	4.0892(2)	3.044(3)	−1.36(2)	19.50
$\mathrm{FP}_{154}^{\text{Type-I}}$	3.95122(5)	3.0567(5)	−1.322(3)	18.81
recommended	3.98263	3.0351	−1.307	18.98

the most accurate to date. For this reason, and with the stipulation that the tubes have been laminated, the glass recipe and supplier[22] are specified[23]. The present measurements may serve as reference data for a specific blend and process of Type-I electric-fusion quartz glass. To this end, recommended values for the fit coefficients to be used with Eq. (2) are given in Table I.

B. Measurement Uncertainty in $\alpha(T)$

From Eq. (2) it is evident that $u[\alpha(T)]$ depends on only two things: how well one measures temperature and length. An uncertainty budget for the present measurement is listed in Table II. Unless otherwise stated, all uncertainties in this work are one standard uncertainty, corresponding to a 68 % confidence level. The notation $u(x)$ is used to denote the standard uncertainty of the quantity x. Before next describing each entry, it is pointed out that for simplicity all entries in Table II have been added in quadrature to produce the combined $u[\alpha(T)]$. However, some entries have no temperature dependence and do not systematically affect $\alpha(T)$. Consequently, the uncertainty in $\int \alpha(T)\,\mathrm{d}T$ using Table II as written would be slightly overestimated. It is also emphasized that Table II only covers measurement uncertainty of a nominal fused quartz glass specimen, and includes no coverage for material inhomogeneity (see Table I and Ref. 11).

The entry "L_{ref}" in Table II refers to the length of the polished-ends tube spacer which forms the FP cavity. The optical length of an FP cavity may be determined within one part in 10^{11} by relating a measured resonance frequency to a mode number (and accounting for diffraction and mirror phase shifts). However, the length of the tube differs from the length of a FP cavity, and corrections are applied for mirror sagitta −49(10) µm, height of the mirror stack +8.0(1) µm, and penetration of the field into the coating −0.55(1) µm. A cosine error related to angular misalignment between the tube bore axis and the axis of the TEM_{00} cavity mode introduces an additional 6 µm uncertainty. Overall, uncertainty in the tube spacer length $u(L_{\text{ref}})$ is a relatively small contributor when the FP cavity length is 333 mm. To be clear, L_{ref} is the tube length at $T_{\text{ref}} = 293.15$ K, and the analysis of thermal expansion uses this reference value in $\alpha(T) = \frac{1}{L_{\text{ref}}}\frac{\mathrm{d}L}{\mathrm{d}T}$.

As mentioned, the FP-based approach to thermal expansion affords tremendous precision in tracking specimen length by inferring changes in cavity length $\mathrm{d}L$ via change in resonant frequency. The uncertainty in measuring a change in resonant frequency is 4 kHz (or, 10^{-11} fractional), imposed by the stability of the iodine-stabilized HeNe laser reference. The entry "frequency" in Table II is negligible compared to other contributors. Rather than the ability to measure a resonant frequency, the measurement of $\mathrm{d}L$ is limited by imperfect materials and other mechanical or optical effects which disguise the temperature-induced length change of the spacer—the thing that is supposed to be measured. These other effects, unrelated to frequency metrology, are described next.

Temporal drift and instability in the cavities was, in fractional terms, 4.5×10^{-11} /d at

TABLE II. Standard uncertainty in measurement of the coefficient of thermal expansion for a nominal fused quartz glass specimen. No coverage for inhomogeneity[11] is included.

component	$u[\alpha(T)]$ /(10^{-10} K^{-1})
L_{ref}, 12 µm	0.2
dL	
frequency, 4 kHz	0.1
instability, 15 pm/d	0.8
mirror mismatch, 80 pm/K	2.4
round-trip phase, 76 kHz/K	1.7
free-spectral range, 17 kHz/K	0.4
dT_{90}	
calibration, 0.1 mK	0.5
stability, 0.5 mK	2.5
self-heat, 0.3 mK	1.5
nonlinearity, 0.3 mK	1.5
gradients, 0.5 mK	2.5
residual gas, 10 mPa	0.2
regression, 149 pm/m	1.5
combined ($k = 1$)	5.4

293.15 K. This estimate is based on a measurement of the change in resonant frequency while the cavities remained at vacuum for five days. Drift in cavity length may be corrected within 10 % across the 17 d of a measurement campaign, resulting in a 8×10^{-11} /K contribution to $u[\alpha(T)]$. This stability assessment is of too short a duration to comment on longer-term effects, nor was there an obvious dependence of temporal stability on temperature, and these facts should be considered when making comparison to other work. That being said, the work of Berthold, Jacobs, and Norton[24] showed drift rates $5.6(3) \times 10^{-10}$ /d and $5.1(3) \times 10^{-10}$ /d for Type-II and Type-III silica glasses, respectively, over six months near 300 K. Excepting modern electronics, the present measurement technique is entirely analogous to Berthold, Jacobs, and Norton[24], but there is a factor 12 discrepancy in drift rates, which has no explanation. As stated above, the body of work by Jacobs and coworkers is very impressive—in Ref. 24, for example, they made great efforts to separate instability in optical contact from instability in the phase shift on reflection, and they also simultaneously measured cavities of different lengths—the work is impressive, but it is unclear how their apparatus[24] achieved frictionless support between the cavity and the chamber. A longer-term study with silica glass of unspecified type by Schödel and Abou-Zeid[25] employed a Twyman-Green large field imaging interferometer. Over seven years at 293.15 K, their sample exhibited a drift rate which slowed annually, ranging from 6.8×10^{-11} /d (initial) to 1.5×10^{-11} /d (final), with a fractional measurement uncertainty of about 4.9×10^{-12}. A third study by Takahashi[26], lasted two years at 293.15 K, and monitored the change in separation between graduations of a line scale deposited on Type-III silica glass. The measurement technique employed a displacement interferometer and microscope, and estimated a fractional drift rate $(0 \pm 4.7) \times 10^{-11}$ /d. The observed short-term drift rates of the present work are consistent with the works of both Schödel and Abou-Zeid[25], and Takahashi[26]. (Note: Refs. 25 and 26 both reported results on a yearly timescale, congruous with the sensitivity of their instruments—their reported data have been converted to a daily timescale.)

Continuing with the subject of cavity length instability, a different effect is now discussed: helium permeation into quartz glass. The present procedure soaked the cavities in 100 Pa of helium gas for 12 h to rapidly equilibrate the glass with the changing bath temperature. In this work there was no evidence that the helium soak adversely affected the $L(T)$ dataset, and an argument may be made, based on past experiences, why no instability was observed. Tests subsequent to Ref. 27 revealed that for three different FP cavities of similar geometry,

fractional increase in and evacuated cavity length inside a block of glass exposed to 100 kPa helium was $2.5(3) \times 10^{-9} \cdot \sqrt{t}$, where t is duration of helium exposure; tests also revealed that the rate of length increase was directly proportional to helium pressure. Older, lower accuracy data presented in Ref. 10 for a much different cavity system whose optical path was helium-filled, shows a $\sqrt{t}$-fractional rate of increase similar to Ref. 27. The present work differs from Refs. 10 and 27 in one important respect: the older works employed cavities made with a binary glass of SiO_2 and 8 % wt TiO_2. On this score, Shelby[28] found no clear dependence on the (helium) permeation coefficient versus concentration of titania for a SiO_2 binary glass (within a 14 % measurement error). Elsewhere, Avdiaj *et al.*[29] measured the permeation coefficient of a SiO_2–TiO_2 binary glass within an uncertainty of 8 %; Avdiaj *et al.* noted that their measurement matched the handbook value for a Type-III fused silica glass within 30 %. The preceding remarks offer good evidence that, for cavities made in fused quartz glass versus a SiO_2–TiO_2 binary glass, changes in cavity length caused by helium permeation would be the same within 20 %. Consequently, a reasonable prediction for cavity length instability may be based upon the older works of SiO_2–TiO_2 binary glasses with helium: one may predict that 12 h exposure to helium at 100 Pa gives rise to fractional instability in cavity length at the level of 8.7×10^{-12}. This prediction is equivalent in magnitude to frequency instability in the iodine-stabilized laser or a 20 µK error in the measurement of glass temperature—at this level, helium soaking does not cause detectable changes in cavity length.

The effect of a potential mismatch in CTE between the mirror and the tube was modeled by the finite-element method. Two mismatch effects come into play[30]: mismatch between the spacer and substrate, and mismatch between the thinfilm coating and the substrate. It was assumed that the mirror CTE was 5×10^{-8} /K larger than the tube CTE; this assumption covers the range of variability in CTE for the vitreous silica glasses shown in Figure 3(d). It was assumed that the CTE of the thinfilm was 1.8×10^{-6} /K; this assumption is an estimate of the mean value of silica and tantala[31,32]. The model showed cavity length to anomalously increase in length by 40 pm/K, with 58 % arising from the thinfilm–substrate mismatch. Within this 40 pm/K anomalous distortion, about 85 % of the effect was a "piston" displacement at the end of the cavity, and the remainder was mirror bending. That is, mirror bending was "outward," increasing cavity length, and contributing a change to the radius of curvature (discussed more in the next paragraph). The present experiment with cavities of dissimilar lengths was purposely conceived to validate this model, but inhomogeneity in $\alpha(T)$ among tubes precluded any assessment; inhomogeneity in $\alpha(T)$ is 54 times larger than the effect of any likely mismatch in $\alpha(T)$ between mirror and tube. The estimate "mirror mismatch" in Table II is therefore model-based, and refers to anomalous displacement at the ends of the specimen only. (Confidence in the finite-element estimates above was bolstered by crossvalidation against the models of Fox[30] and Legero, Kessler, and Sterr[33]. It is emphasized that the estimates are specific to the present geometry: tube 18 mm outer diameter, inner diameter of tube bore at mirror contact 12 mm, mirror substrate diameter 25 mm, substrate thickness 10 mm, thinfilm coating diameter 8 mm, coating thickness 2 µm. As an example of the geometry dependence, mirror bending increases by a factor of 26 if the substrate were only 1 mm thick.)

Contributors arising from the simplified FP cavity resonance frequency are included in the entry "round-trip phase." The complete expression for a resonance frequency $\nu = \frac{c}{2L}\left[m + \frac{\Phi_G(L)}{\pi} - \frac{\phi_R(\nu)}{\pi}\right]$ accounts for the Gouy phase shift and the phase shift on reflection. The Gouy phase $\Phi_G = \arcsin[(L/R)^{1/2}]$ depends on cavity length L and the mirror radius of curvature R; it arises from the difference in on-axis phase accumulated by a Gaussian beam versus a planar wavefront. The phase shift on reflection ϕ_R is given by the argument of the complex reflection coefficient from the dielectric mirror stack. The reflected phase depends on the properties of the stack (e.g., thinfilm thickness and refractive index), and may be calculated by the transfer-matrix method[34]. Instead of $\frac{dL}{L} = -\frac{d\nu}{\nu}$, a more exact

estimate for change in cavity length inferred by a change in resonance frequency

$$\frac{\Delta L}{L} = \frac{\Delta\nu + \dfrac{c}{2L(T)}\left[\Delta m + \dfrac{\Phi_{\mathrm{G}}(T) - \phi_{\mathrm{R}}(T)}{\pi}\right]}{\nu}, \tag{4}$$

takes into consideration a temperature dependence in both these round-trip phase terms—Φ_{G} and ϕ_{R}. For the Gouy phase shift, the temperature-induced cavity length change is approximately 0.4 (µm/m)/K, and therefore contributes $\frac{\mathrm{d}}{\mathrm{d}T}\Phi_{\mathrm{G}} = 0.28$ µrad/K to round-trip phase in the long cavity. Additionally, the finite-element model for a mismatch in tube–mirror CTE (previous paragraph) predicted an increase in sagitta $\frac{\mathrm{d}s}{\mathrm{d}T} = 4$ pm/K; assuming the concave portion of the mirror forms a chord of length l between the bonded annulus, the outward bending mirror contributes to a changing radius of curvature $\frac{\mathrm{d}R}{\mathrm{d}T} \approx -\frac{\mathrm{d}s}{\mathrm{d}T}\frac{l^2}{8s^2}$, or 0.3 µm/K and $\frac{\mathrm{d}}{\mathrm{d}T}\Phi_{\mathrm{G}} = 0.64$ µrad/K. In terms of resonant frequency, the net result on Gouy phase for temperature-induced changes in cavity length and radius of curvature is 100 Hz/K, which is a negligible effect. The temperature dependence of the phase-shift on reflection is more significant. A model of the mirror stack calculated[34] changes in ϕ_{R} (at fixed wavelength) as a function of temperature. The layers of the mirror stack were perturbed for the effects of the thermooptic $\frac{\mathrm{d}n}{\mathrm{d}T}$ and thermal expansion $\frac{\mathrm{d}L}{\mathrm{d}T}$ coefficients[31], and the model predicted $\frac{\mathrm{d}}{\mathrm{d}T}\phi_{\mathrm{R}} = 0.56$ mrad/K as the combined effect of two mirrors. The temperature dependence of $\phi_{\mathrm{R}}(T)$ means that there is a systematic error of up to 80 kHz/K in the dataset for the long cavity specimen, and 178 kHz/K for the short specimens. Additionally, the group delay $\tau = \frac{1}{2\pi}\frac{\mathrm{d}\phi_{\mathrm{R}}}{\mathrm{d}\nu}$ also exhibited a temperature dependence $\frac{\mathrm{d}}{\mathrm{d}T}\tau = 0.2$ as/K. The effect of $\frac{\mathrm{d}}{\mathrm{d}T}\tau$ causes a pseudorandom error in the estimate of ΔL, the magnitude of which depends on the value of the measured change in beat frequency Δf. In all datasets, 68 % of the Δf measurements fall within (180±330) MHz, and since $\frac{\mathrm{d}\nu}{\mathrm{d}T} \approx 189$ MHz/K together with the average $\mathrm{d}T = 3.1$ K in the procedure, one might expect random errors of ±231 pm/m to appear in the datasets, uncorrelated between the cavities. In Figure 3(b) there is no evidence of uncorrelated residuals this large, which suggests that the thinfilm perturbations[31] to the mirror model are overestimated. Ref. 31 states that thermal properties of thinfilms are not very well known—measurements are scarce, thinfilm properties are believed to be considerably different than bulk material, and there is some ambiguity about the sign when there is a material property mismatch between the film and substrate. In any case, current knowledge of thinfilm properties precludes any attempt at correcting for systematic or pseudorandom effects, and the entry in Table II expresses the inability to correct for $\phi_{\mathrm{R}}(T)$.

The preceding paragraph revealed the fact that the change in resonant frequency has a modulo-$\frac{c}{2L}$ component. The present estimate of the cavity length L is based on a measurement of free-spectral range $\Delta\nu_{\mathrm{FSR}} = \frac{c}{2L}(1+\epsilon_\tau)$, with $\epsilon_\tau = \frac{c\tau}{L}$ and $\tau = \frac{1}{2\pi}\frac{\mathrm{d}\phi}{\mathrm{d}\nu}$ being the group delay. In the present work, residual-amplitude modulation in the laser systems was not canceled, and the present estimate of $\Delta\nu_{\mathrm{FSR}}$ is no better than 1 kHz for the long cavity, or about 2×10^{-5} in fractional terms. Uncertainty in ϵ_τ is twenty times smaller than this. The laser locked to the long cavity was tuned to a different resonant cavity mode number every 1.7 K on average. Consequently, error in the $\Delta\nu_{\mathrm{FSR}}$-inferred value of cavity length causes a scale error of 17 kHz/K, but the entry in Table II for free-spectral range shows it to be a small contributor overall.

Uncertainty in the temperature of the cavities is in sum the largest contributor to $u[\alpha(T)]$. Before summarizing each entry comprising $u(\mathrm{d}T_{90})$, it is mentioned that the present measurements are reported on the international temperature scale of 1990 (ITS-90), and consequently are in error[35] by about 6 mK across the $(263 < T < 313)$ K temperature range of interest—temperature-scale error is about 12 times larger than any other contributor to $u(\mathrm{d}T_{90})$. So, noting that Table II does not include an uncertainty estimate for $T - T_{90}$, the other temperature-related entries are briefly described. The master thermometer to which the thermistors were compared was a capsule-type standard platinum resistance thermometer which had been calibrated on ITS-90; the uncertainty in the ITS-90 fixed points is

0.1 mK. History on this particular cSPRT indicate that its calibration coefficients are no more stable than 0.5 mK over six months. The thermometer bridge used to measure the resistors has a specified nonlinearity in the measurement corresponding to 0.3 mK for this temperature-resistance ratio range. To correct for a temperature-dependence in resistive heating ("self-heating"), all temperature measurements were referenced to zero power, but the present confidence in the correction is no better than 0.3 mK.

Finally, the last uncertainty contributor related to $\mathrm{d}T_{90}$ is a temperature gradient between the glass specimens and the thermometer. Two thermistors were used to measure gradients between opposite corners of the two aluminum cavity suspension enclosures shown in Figure 2. Two thermopiles were used to measured gradients between the suspension enclosures and the isothermal flange (which housed the cSPRT) shown in Figure 2. Between the redundancy of two thermistors and two thermopiles, gradients were detected within 0.3 mK. Nevertheless, the suspension enclosure is not the glass cavity, and this is relevant because the measurement technique is quasi-dynamic—100 Pa of helium was used to rapidly equilibrate the system during a temperature change, and pumping this gas out to measure the cavities at vacuum induced gradients up to 2 mK between the isothermal flange and (colder) suspension enclosure. The glass–aluminum system of Figure 2 approaches full concentric enclosure, where radiative heat transfer[36] between the two surfaces would be written $Q = A_1\sigma(T_1^4 - T_2^4)/[\frac{1}{\epsilon_1} + \frac{A_1}{A_2}(\frac{1}{\epsilon_2} - 1)]$, with the areas of glass and aluminum A_1 and A_2, temperatures T_1 and T_2, emissivities ϵ_1 and ϵ_2, respectively. When $T_1 - T_2 < 10$ mK, the series approximation $T_1^4 - T_2^4 = 4(T_1 - T_2)T_2^3 + \cdots$ is fractionally accurate within 10^{-4} near ambient. The energy balance between radiative Q and the cavity body rate of heat transfer $\rho V c_p \frac{\mathrm{d}T}{\mathrm{d}t}$ then prescribes a thermal time constant $\tau = \frac{\rho V c_p}{4A_1\sigma T_2^3}[\frac{1}{\epsilon_1} + \frac{A_1}{A_2}(\frac{1}{\epsilon_2} - 1)]$, with glass density ρ, volume V, and specific heat c_p. This approximate model estimates $\tau = 1.8$ h. Since there was a 12 h wait between helium pump-out and acquiring a $L(T)$ data point, and since the system temperature is stable within 0.5 mK in that time frame, any few millikelvin gradients between the aluminum and glass created by pV work would be well under 0.5 mK after 6 time constants. Assigning an uncertainty of 0.5 mK to undetected gradients is therefore overcautious—especially since steady-state gradients measured between ends of the two aluminum enclosures were always less than (0.22 ± 0.15) mK—but this reflects the lack of comfort on this point: actual glass temperature was not measured, rather a low-emissivity body enclosing the glass, in vacuum, which had been cooled from pV-work.

The bath and plumbing system employed was optimized for thermal performance, and openings in the thermal shells are few and small. This approach is at odds with good vacuum practice. For the CTE measurements, a 50 mm outer diameter vacuum hose was run into the bath, but the chamber was pumped through a 17 mm inner diameter flange. Ultimate vacuum inside the chamber was no better than 40(10) mPa. Steady-state residual gas is not an error, but pressure fluctuations change the refractive index between the cavity mirrors, and this change in optical length would be an error, if unaccounted for. Chamber pressure was continuously monitored with a diaphragm gage: measurement indicated residual pressure did not fluctuate by more than 10 mPa. The residual pressure was most likely water vapor, but small amounts of helium would also be present: not enough was known about its molar refraction to apply corrections to the resonance frequency. Assuming worst case of 10 mPa fluctuation of water vapor, CTE measurements in the long FP cavity would have errors of about 8 pm caused by changes in refractive index, corresponding to 2×10^{-11} /K in α, if measured across 1 K. The entry "residual gas" in Table II is therefore overestimated for the interest of scaling cell length over 20 K.

The entry "regression" in Table II is the quadrature sum of the root-mean-square error in the fit plus error in the fit model. Each of these components is now explained in turn. The residuals from the $\frac{L(T)}{L_{\mathrm{ref}}}$ fit are plotted in Figure 3(b). Note that these residuals exceed the present detection limit for a change in cavity length by more than an order of magnitude. The most likely explanation for the residuals, correlated in long and short cavities, is systematic error in measuring the cavity temperatures, on the order of 0.28 mK. As the previous entry for $u(\mathrm{d}T_{90})$ shows, present confidence in thermometry is no better than 0.8 mK, and

so the magnitude of the residuals is not surprising. The second (larger) component added in quadrature with the residuals is uncertainty in the fit model, and requires a brief preface. In literature there are different approaches to fit or deduce $\alpha(T)$. In the field of metrology, it has been customary to fit with polynomials[4,8,12,16,21]. Some recognize the correlation between thermal expansion and heat capacity via the Grüneisen parameter[37–39], and from there go on to recommend fitting based on an Einstein model with "empirical pseudo-quasi-harmonic [phonon] modes"[40–42]; or, when describing mid-range temperatures, functions with fewer free parameters[43]. Indeed, Reeber and Wang[41] explicitly advise against polynomials because they do not reliably extrapolate. Others take a hybrid approach, invoking an Einstein solid plus something else to describe low-temperature behavior—a quadratic term in the case of Swenson[44], and a Schottky-like function by Okaji[14]. The preceding remarks are but cursory: their purpose was to draw attention to the fact that there are several models to describe $\alpha(T)$, and thence with which to fit $L(T)$. The choice of fit model becomes preponderant in high-accuracy work because as Martin, Bartl, and Elster[45] point out, extracting $\alpha(T)$ is an ill-posed problem, since it is based on a derivative; consequently, the choice of model might lead to different answers for $\alpha(T)$. Martin, Bartl, and Elster report a model-dependent deviation of up to 1×10^{-9} /K when deducing thermal expansion from measured $L(T)$ data in a silicon specimen. In the present case, even in this limited temperature range, it was found that two pseudo-quasi-harmonic modes[41] are required to fit $\frac{L(T)}{L_{\text{ref}}} = b_0 + \sum_{i=1}^{2} X_i \Theta_i / [\exp(\Theta_i/T) - 1]$, and describing

$$\alpha(T) = \sum_{i=1}^{2} X_i \left(\frac{\Theta_i}{T}\right)^2 \frac{\exp(\Theta_i/T)}{[\exp(\Theta_i/T) - 1]^2}, \tag{5}$$

requires four terms

$$\begin{aligned} X_1 &= -1.20(4) \times 10^{-6}\ /\text{K} \qquad \Theta_1 = 8.4(3)\ \text{K} \\ X_2 &= 2.14(4) \times 10^{-6}\ /\text{K} \qquad \Theta_2 = 549(6)\ \text{K}, \end{aligned}$$

instead of the three terms of the quadratic in Eq. (2). It is thus unclear what benefit a pseudo-quasi-rigorous regression offers in this situation. [Insofar as the fit parameters of Eq. (5) are physically meaningful, Θ_2 is related to the Debye temperature. Stephens[46] reported a Debye temperature of 494(25) K by measurement of the heat capacity of fused quartz glass. Okaji[14] inferred 535(9) K via measurement of CTE; their approach regressed $\alpha(T)$ and not $L(T)$, and the first term of their fit function differed from Eq. (5).] In concurrence with the work of Martin, Bartl, and Elster[45], it was found that Eq. (5) differs from the polynomial Eq. (2) by 1.2×10^{-10} /K standard deviation, which in fractional terms is $2.9 \times 10^{-4} \cdot \alpha(T)$—consistent with the $3 \times 10^{-4} \cdot \alpha(T)$ finding of Ref. 45 for silicon. For the ultimate interest $\int \alpha(T)\,\mathrm{d}T$, the difference between the models is less than 0.6 nm/m, which is a negligible concern. The entry "regression" in Table II is half the span of the fit model error added in quadrature with the root-mean-square error of the residuals from the fit.

To conclude, $u[\alpha(T)]$ listed in Table II has several contributors of similar magnitude, at the level of a few 10^{-10} /K. Some of these have been incurred because the apparatus employs vacuum and thermal systems which was not designed for the purpose of CTE measurement. A different apparatus may be imagined, with greatly reduced chamber volume, increased vacuum conductance, and a thermal spray on all aluminum surfaces to increase emissivity. Such improvements might reduce $u[\alpha(T)]$ by about 40 %. However, breaking the 3×10^{-10} /K threshold appears challenging—it would require an understanding of thinfilm coatings and reflected phase shift beyond state-of-the-art.

C. Uncertainty Scaling L_{CMM} for Temperature

The previous subsection has discussed measurement uncertainty for a nominal fused quartz glass specimen. However, for the ultimate interest scaling L_{CMM} for temperature,

the uncertainty budget of Table II has almost no relevance—$u[\alpha(T)]$ is 24 times smaller than inhomogeneity among the tubes. Instead, uncertainty scaling L_{CMM} for temperature is dominated by the information provided in Figure 3(c) and Table I, which are now discussed in more detail.

Figure 3(c) is an intercomparison of four specimens, with the specimen $\mathrm{FP}_{333}^{\text{Type-I}}$ acting as the check standard. The additional specimen $\mathrm{FP}_{154}^{\text{Type-I}}$ was briefly mentioned. Its creation was reactionary to the initial finding of large inhomogeneity. From Figure 3(c) and recognizing $\Delta\alpha \approx \frac{1}{\nu}\frac{\Delta f_{\mathrm{beat}}}{\Delta T}$ relative to the check standard $\mathrm{FP}_{333}^{\text{Type-I}}$, the specimen $\mathrm{FP}_{152}^{\text{Type-I}}$ exhibits a difference in $\alpha(T)$ of $+1.1 \times 10^{-8}$ /K, and the specimen $\mathrm{FP}_{154}^{\text{Type-I}}$ exhibits a difference of -0.2×10^{-8} /K. So the range of inhomogeneity among three tube specimens is $\Delta\alpha = 1.3 \times 10^{-8}$ /K. (Alternately, these estimates of $\Delta\alpha$ can be obtained in the final column $\frac{\Delta L}{L}$ of Table I, recognizing $\Delta T = 50$ K.) These tests of three specimens are not sufficient to make sound statistical inferences, but the work of Jacobs, Shough, and Connors[11] is again mentioned. They showed $\Delta\alpha = 1.3 \times 10^{-8}$ /K among thirteen specimens. Based on the three measured specimens in the present work, supported by the more thorough study of Jacobs, Shough, and Connors[11], it is felt that taking half the range $\Delta\alpha = 1.3 \times 10^{-8}$ /K is a reasonable decision. So, half the range of the three specimens measured is thought to cover inhomogeneity among all tubes used to make the gas cells, at the 68 % confidence level.

Next from Figure 3(c) is that relative to the check standard $\mathrm{FP}_{333}^{\text{Type-I}}$, the short cavity specimen increased by $\Delta\alpha = 0.2 \times 10^{-8}$ /K when it was modified from $\mathrm{FP}_{152}^{\text{Type-I}}$ to $\mathrm{FP}_{152}^{\text{potted}}$. This finding is not unexpected, because the potting compound has a generic mean CTE specification of 0.59×10^{-6} /K. Covering uncertainty for the effect of potting compound therefore uses this measurement together with a length dependence, because the total "length" of compound used to pot the tube of $\mathrm{FP}_{152}^{\text{potted}}$ was 60 mm, whereas the medium and long gas cells have 50 mm of their ends potted in compound. The measured change between $\mathrm{FP}_{152}^{\text{Type-I}}$ and its potted $\mathrm{FP}_{152}^{\text{potted}}$ gives a high level of confidence that the potting compound increases the effective thermal expansion of the gas cells. However, the somewhat uncontrolled nature of potting tubes (quantity used, layer thickness, squeeze out) means that a large uncertainty should be assigned to the effect. Specifically, for the 0.5 m cell which has 50 mm of each tube-end potted, the estimate is that the potting compound increases effective CTE by $7.0^{+7.0}_{-0.0} \times 10^{-10}$ /K.

The final uncertainty estimate scaling L_{CMM} for temperature is therefore the quadrature sum of CTE measurement uncertainty from Table II, plus the effect of the potting compound, together with half the range of measured inhomogeneity; so that $u[\alpha_{\mathrm{cell}}(T)]$ is 6.6×10^{-9} /K, in which inhomogeneity dominates.

III. CONCLUSION

To conclude by clarification: this work does not advocate for fused quartz glass as a standard of thermal expansion—Figure 3(d) is a strong case against such an endeavor. The thermal-expansion measurements reported here are merely an attendant outcome of the quest to know L_{cell} at 273.16 K, with the goal of establishing an optical pressure scale at the accuracy level of 1 µPa/Pa. The quest has been thoroughly justified: if cell length had been scaled for thermal expansion using the mean of Refs. 4, 13, and 14, the consequence for the optical pressure scale would have been a bias error of at least 1.5 µPa/Pa, with an underestimated uncertainty for $u(L_{\mathrm{cell}})$.

Appendix A: Supplementary Information

The supplementary material to this article is available on the NIST public data repository: https://doi.org/10.18434/mds2-2697. The supplementary material is an archive file,

containing three sets of measurement data, which are:

- Set 1: specimens $\mathrm{FP}_{333}^{\text{Type-I}}$ and $\mathrm{FP}_{152}^{\text{Type-I}}$ cycled in temperature side by side.
- Set 2: specimens $\mathrm{FP}_{333}^{\text{Type-I}}$ and $\mathrm{FP}_{152}^{\text{potted}}$ cycled in temperature side by side.
- Set 3: specimens $\mathrm{FP}_{333}^{\text{Type-I}}$ and $\mathrm{FP}_{154}^{\text{Type-I}}$ cycled in temperature side by side.
- A Python script is included which reproduces Figure 3, and also contains the historical reference data.

[1] K. Jousten, "A unit for nothing," Nature Physics **15**, 618 (2019).
[2] M. Puchalski, K. Piszczatowski, J. Komasa, B. Jeziorski, and K. Szalewicz, "Theoretical determination of the polarizability dispersion and the refractive index of helium," Physical Review A **93**, 032515 (2016).
[3] P. F. Egan, J. A. Stone, J. E. Ricker, J. H. Hendricks, and G. F. Strouse, "Cell-based refractometer for pascal realization," Optics Letters **42**, 2944–2947 (2017).
[4] T. A. Hahn and R. K. Kirby, "Thermal expansion of fused silica from 80 to 1000 K—Standard Reference Material 739," AIP Conference Proceedings **3**, 13–24 (1972).
[5] J. Oishi and T. Kimura, "Thermal expansion of fused quartz," Metrologia **5**, 50–55 (1969).
[6] R. Brückner, "Properties and structure of vitreous silica. I," Journal of Non-Crystalline Solids **5**, 123–175 (1970).
[7] E. G. Wolff and S. A. Eselun, "Thermal expansion of a fused quartz tube in a dimensional stability test facility," Review of Scientific Instruments **50**, 502–506 (1979).
[8] H. Wang, N. Yamada, and M. Okaji, "Precise dilatometric measurements of silica glasses," Netsu Bussei **13**, 17–22 (1999).
[9] S. F. Jacobs, J. N. Bradford, and J. W. Berthold, "Ultraprecise measurement of thermal coefficients of expansion," Applied Optics **9**, 2477–2480 (1970).
[10] P. Egan and J. A. Stone, "Absolute refractometry of dry gas to ±3 parts in 10^9," Applied Optics **50**, 3076–3086 (2011).
[11] S. F. Jacobs, D. Shough, and C. Connors, "Thermal expansion uniformity of materials for large telescope mirrors," Applied Optics **23**, 4237–4244 (1984).
[12] K. P. Birch, "An automatic absolute interferometric dilatometer," Journal of Physics E: Scientific Instruments **20**, 1387–1392 (1987).
[13] W. D. Drotning, "A laser interferometric dilatometer for low-expansion materials," International Journal of Thermophysics **9**, 849–860 (1988).
[14] M. Okaji, N. Yamada, K. Nara, and H. Kato, "Laser interferometric dilatometer at low temperatures: application to fused silica SRM 739," Cryogenics **35**, 887–891 (1995).
[15] H. Wang, N. Yamada, and M. Okaji, "Thermal expansion of some silica glasses in the range from −50 to 250 °C by push-rod dilatometry," in *Thermal Conductivity 25*, edited by C. Uher and D. Morelli (Technomic Publishing Company, 2000) pp. 49–57.
[16] M. Okaji and K. P. Birch, "Intercomparison of interferometric dilatometers at NRLM and NPL," Metrologia **28**, 27–32 (1991).
[17] A. Rohatgi, "Webplotdigitizer: Version 4.4," (2020).
[18] J. W. Berthold and S. F. Jacobs, "Ultraprecise thermal expansion measurements of seven low expansion materials," Applied Optics **15**, 2344–2347 (1976).
[19] S. F. Jacobs and D. Shough, "Thermal expansion uniformity of Heraeus-Amersil TO8E fused silica," Applied Optics **20**, 3461–3463 (1981).
[20] J. Burge, T. Peper, and S. Jacobs, "Thermal expansion of borosilicate glass, Zerodur, Zerodur M, and unceramized Zerodur at low temperatures," Applied Optics **38**, 7161–7162 (1999).
[21] S. J. Bennett, "An absolute interferometric dilatometer," Journal of Physics E: Scientific Instruments **10**, 525–530 (1977).
[22] Heraeus Quarzglas, Lamp Quality HLQ270, electric fusion process. Typical impurities: Li = 0.05 µg/g, Na = 0.05 µg/g, K = 0.1 µg/g, Mg = 0.05 µg/g, Ca = 0.5 µg/g, Fe = 0.1 µg/g, Cu < 0.05 µg/g, Cr < 0.05 µg/g, Mn < 0.05 µg/g, Al = 15 µg/g, Ti = 1.1 µg/g.
[23] Certain equipment, instruments, software, or materials, commercial or non-commercial, are identified in this paper in order to specify the experimental procedure adequately. Such identification is not intended to imply recommendation or endorsement of any product or service by NIST, nor is it intended to imply that the materials or equipment identified are necessarily the best available for the purpose.
[24] J. W. Berthold, S. F. Jacobs, and M. A. Norton, "Dimensional stability of fused silica, Invar, and several ultra-low thermal expansion materials," Metrologia **13**, 9–16 (1977).
[25] R. Schödel and A. Abou-Zeid, "High accuracy measurements of long-term stability of material with PTB's precision interferometer," in *Fifth International Symposium on Instrumentation Science and Technology*, Vol. 7133, edited by J. Tan and X. Wen, International Society for Optics and Photonics (SPIE, 2009) pp. 903–911.
[26] A. Takahashi, "Long-term dimensional stability and longitudinal uniformity of line scales made of glass ceramics," Measurement Science and Technology **21**, 105301 (2010).

[27]P. F. Egan, J. A. Stone, J. H. Hendricks, J. E. Ricker, G. E. Scace, and G. F. Strouse, "Performance of a dual Fabry–Perot cavity refractometer," Optics Letters **40**, 3945–3948 (2015).
[28]J. E. Shelby, "Helium migration in TiO_2–SiO_2 glasses," Journal of the American Ceramic Society **55**, 195–197 (1972).
[29]S. Avdiaj, Y. Yang, K. Jousten, and T. Rubin, "Note: Diffusion constant and solubility of helium in ULE glass at 23 °C," The Journal of Chemical Physics **148**, 116101 (2018).
[30]R. W. Fox, "Temperature analysis of low-expansion Fabry–Perot cavities," Optics Express **17**, 15023–15031 (2009).
[31]G. H. Ogin, *Measurement of Thermo-Optic Properties of Thin Film Dielectric Coatings*, Ph.D. thesis, California Institute of Technology (2013), page 21 and references therein.
[32]M. R. Abernathy, J. Hough, I. W. Martin, S. Rowan, M. Oyen, C. Linn, and J. E. Faller, "Investigation of the Young's modulus and thermal expansion of amorphous titania-doped tantala films," Applied Optics **53**, 3196–3202 (2014).
[33]T. Legero, T. Kessler, and U. Sterr, "Tuning the thermal expansion properties of optical reference cavities with fused silica mirrors," Journal of the Optical Society of America B **27**, 914–919 (2010).
[34]T. A. Germer, "pySCATMECH: a Python interface to the SCATMECH library of scattering codes," in *Reflection, Scattering, and Diffraction from Surfaces VII*, Vol. 11485, edited by L. M. Hanssen, International Society for Optics and Photonics (SPIE, 2020) pp. 43–54.
[35]J. Fischer, M. de Podesta, K. Hill, M. Moldover, L. Pitre, R. Rusby, P. Steur, O. Tamura, R. White, and L. Wolber, "Present estimates of the differences between thermodynamic temperatures and the ITS-90," International Journal of Thermophysics **32**, 12–25 (2011).
[36]J. R. Howell, M. P. Mengüç, and R. Siegel, "Thermal radiation heat transfer," (CRC Press, Boca Raton, Florida, 2016) Chap. 6, pp. 273–337, 6th ed.
[37]J. B. Wachtman Jr., T. G. Scuderi, and G. W. Cleek, "Linear thermal expansion of aluminum oxide and thorium oxide from 100° to 1100°K," Journal of the American Ceramic Society **45**, 319–323 (1962).
[38]H. Ibach, "Thermal expansion of silicon and zinc oxide (I)," Physica Status Solidi B **31**, 625–634 (1969).
[39]G. Grimvall, "Thermophysical properties of materials," (Elsevier Science B.V., Amsterdam, 1999) Chap. 13, pp. 200–218.
[40]R. R. Reeber, "Thermal expansion of some group IV elements and ZnS," Physica Status Solidi A **32**, 321–331 (1975).
[41]R. R. Reeber and K. Wang, "Thermal expansion and lattice parameters of group IV semiconductors," Materials Chemistry and Physics **46**, 259–264 (1996).
[42]T. Middelmann, A. Walkov, G. Bartl, and R. Schödel, "Thermal expansion coefficient of single-crystal silicon from 7 K to 293 K," Physical Review B **92**, 174113 (2015).
[43]I. Suzuki, S. Okajima, and K. Seya, "Thermal expansion of single-crystal manganosite," Journal of Physics of the Earth **27**, 63–69 (1979).
[44]C. A. Swenson, "Recommended values for the thermal expansivity of silicon from 0 to 1000 K," Journal of Physical and Chemical Reference Data **12**, 179–182 (1983).
[45]J. Martin, G. Bartl, and C. Elster, "Application of Bayesian model averaging to the determination of thermal expansion of single-crystal silicon," Measurement Science and Technology **30**, 045012 (2019).
[46]R. B. Stephens, "Intrinsic low-temperature thermal properties of glasses," Physical Review B **13**, 852–865 (1976).